International Journal of Biological Macromolecules 299 (2025) 140213

Contents lists available at ScienceDirect

International Journal of Biological Macromolecules

journal homepage: www.elsevier.com/locate/ijbiomac

Effect of nanocomposite chitosan/hydroxyapatite pH-induced hydrogels on the osteogenic differentiation of spheroids from adipose stem cells

A.B. Di Stefano [a,1], C. Di Marco [b,1], F. Toia [a,c,*], M. Trapani [a], M. Testa [b], S. Di Leonardo [d], G. Burriesci [d,e], M. Franza [c], E. Cammarata [c], A. Cordova [a,c], F. Lopresti [b], V. La Carrubba [b]

[a] BIOPLAST-Laboratory of BIOlogy and Regenerative Medicine-PLASTic Surgery, Department of Precision Medicine in Medical, Surgical and Critical Care, University of Palermo, Italy
[b] Department of Engineering, University of Palermo, Palermo, Italy
[c] Unità di Chirurgia Plastica e Ricostruttiva, Department of Precision Medicine in Medical, Surgical and Critical Care, University of Palermo, Italy
[d] Bioengineering Group, Ri.MED Foundation, Palermo, Italy
[e] UCL Mechanical Engineering, University College London, Torrington Place, London WC1E 7JE, United Kingdom

ARTICLE INFO

Keywords:
Nanocomposite hydrogels
Chitosan
Hydroxyapatite
Spheroids of adipose stem cells
Osteogenic differentiation

ABSTRACT

Chitosan is gaining scientific recognition as a hydrogel in bone tissue engineering (BTE) due to its ability to support osteoblast attachment and proliferation. However, its low mechanical strength and lack of structural integrity limit its application. Nanometric hydroxyapatite (HA) is used as a filler to enhance the mechanical properties and osteoinductivity of hydrogels. In this study, chitosan-based hydrogels were systematically compared by adding 10 %, 20 %, and 30 % HA to evaluate their impact on chemical-physical properties and cellular behavior. Mechanical reinforcement of HA was evaluated by rheological and mechanical tests, with results showing a marked increase in stiffness and mechanical strength as HA concentration increased. Specifically, the Young's modulus and the compression strength increased from 26.8 kPa for chitosan alone to 63.8 kPa and with values reaching 183 kPa for the 30 wt% HA sample. Swelling tests revealed a decrease in water absorption with higher HA concentrations, while weight loss measurements showed that the addition of HA improved hydrogel stability. Biological analysis demonstrated that stem cells maintained viability, with osteopontin expression observed after 14 days of culture, indicating successful differentiation toward osteoblasts. This study highlights the significant potential of HA-enhanced chitosan hydrogels for BTE applications, with improved mechanical properties and osteoinductive capabilities.

1. Introduction

Three-dimensional (3D) culture systems provide an innovative approach to tissue engineering and regenerative medicine by better replicating the complexity of *in vivo* tissues. Two-dimensional (2D) cell cultures do not accurately mimic the complex 3D architecture and microenvironment of native tissues. This limitation is particularly relevant in the context of osteogenic differentiation, where the 3D microenvironment plays a critical role in influencing cell behavior, including proliferation, migration and differentiation. While 3D cell culture models, such as spheroids, closely mimic *in vivo* conditions by providing the necessary cell-to-cell and cell-to-matrix interactions, their integration with materials, such as nanocomposite hydrogels, has been relatively underexplored. Compared to traditional two-dimensional (2D) cultures, these devices more accurately mimic the complexity of *in vivo* tissues. Currently, millions of patients suffer from bone defects resulting from congenital factors, trauma, inflammation, and tumors [1]. The primary challenge in orthopedics is addressing significant bone defects, mainly due to the complexity of the bone regeneration process [2]. The regeneration capacity of auto/allografts has produced interest in exploring alternative approaches for bone tissue engineering (BTE) [3]. Bone is a connective tissue with a mineralized extracellular matrix (ECM), which consists of 60 % inorganic material, such as hydroxyapatite, 10 % water, and 30 % organic components such as type I collagen fibers [4,5]. Developing scaffolds that mimic natural bone tissue for bone tissue engineering (BTE) requires osteoinductive properties. This

* Corresponding author at: Plastic and Reconstructive Surgery, Department of Precision Medicine in Medical, Surgical and Critical Care, University of Palermo, via Liborio Giuffrè, 5, 90127 Palermo, Italy.
[1] These authors equally contributed to the work.

https://doi.org/10.1016/j.ijbiomac.2025.140213
Received 28 October 2024; Received in revised form 10 January 2025; Accepted 20 January 2025
Available online 22 January 2025

means that the scaffold should have the ability to promote osteogenesis and bone formation. Furthermore, the scaffold must be biocompatible, biodegradable, and provide mechanical support such as compressive strength. It is also relevant that the scaffold exhibits a high degree of pore interconnectivity to facilitate cell distribution and attachment [6]. In addition to the material used, the correct cell type is crucial for BTE [7]. Mesenchymal stem cells (MSCs) are widely used for this purpose due to their high osteoinductivity and osteogenic potential. They can be easily isolated from different tissues such as bone marrow (BMSCs) or adipose tissue (ASCs) [8–10]. ASCs are obtained from adipose tissue *via* liposuction, a safe and non-invasive procedure, and its allogeneic use is possible with a low risk of immunogenicity. For this reason, ASC-based therapy is promising and could replace bone grafts [8,11]. MSCs are commonly cultured as a two-dimensional (2D) monolayer, but to reproduce the *in vivo* microenvironment more accurately *in vitro*, three-dimensional (3D) culture systems have been developed [12,13]. Three-dimensional cellular spheroids, called spheroids of adipose stem cells (SASCs) a spontaneous assembly of suspended cells, have received attention as they offer unique biological properties [14] such as strong cell-cell and cell-extracellular matrix (ECM) interactions [15]. For example, Saburina et al. [16] reported that ASCs spheroids express osteoblast markers and have angiogenic potential and calcium deposited. In addition, SASCs have been shown to enable bone regeneration *in vivo* when seeded above in a study where laminectomy was performed in mouse models [17] or after calvaria injury in rat models [18] as well as possessing significant immunomodulatory capabilities [19].

In the context of BTE, hydrogel scaffolds play a key role by providing a supportive three-dimensional environment for cell growth, proliferation, and differentiation [20]. Hydrogels are 3D cross-linked hydrophilic polymer networks that can absorb and retain a significant amount of water within their structure. They are able to mimic the ECM due to their high water content. Commonly used hydrogel materials for BTE include natural polymers such as collagen, chitosan, alginate, and hyaluronic acid [21,22], as well as synthetic polymers such as polyvinyl alcohol (PVA) as reported by Xiang C. and colleagues [3]. Natural polymers are suitable due to their excellent biocompatibility, low toxicity, and biodegradability [24]. In addition to natural and synthetic polymers, composite hydrogels, such as such as PCL fibers/GelMA-based systems, are also widely used for their enhanced properties, including controlled release capabilities, as demonstrated in recent studies [25]. In BTE, chitosan (Chi) scaffolds are a promising alternative due to their biocompatibility, biodegradability, osteoinductivity, and antimicrobial properties [26,27]. Chitosan is a natural linear amino polysaccharide, derived from the deacetylation of chitin [28], insoluble in water but able to form a solution in an acidic media. In fact, due to the protonation of amino groups, chitosan becomes positively charged in an acidic aqueous solution. If a strong base such as NaOH is added to the solution, it reacts with the acid protons, neutralizing the solution and deprotonating the amino groups, resulting in the formation of a hydrated gel-like precipitate [21,29–33]. In bone tissue engineering, hydroxyapatite is often used as a nanofiller for chitosan hydrogels due to its biocompatibility and osteoinductivity and acts as a mechanical reinforcement [34–39]. Studies have demonstrated that composite hydrogels based on biopolymers such as chitosan that incorporates HA exhibit enhanced mechanical properties and cell-supporting functions, making them highly effective in bone tissue engineering applications [40].

The use of HA-loaded composite hydrogels has been shown to not only enhance the structural integrity of scaffolds but also to provide a sustained release of bioactive factors that promote bone regeneration. This combination of HA's biological activity with the advantageous properties of chitosan-based hydrogels represents a promising approach for developing scaffolds that can facilitate bone healing, support cell infiltration, and enhance tissue integration [41]. Recently, Yiqun et al. [42] reported that MSCs cultured in 3D chitosan - nanohydroxyapatite hydrogel promoted osteogenic differentiation, Kong et al. [43] reported that chitosan - nanohydroxyapatite scaffold showed better biomineral activity than chitosan hydrogel for BTE.

The primary aim of this study is to compare the effect of three different HA concentrations (10 wt%, 20 wt%, and 30 wt%) on the biological and chemical-physical properties of chitosan-based hydrogels produced *via* pH-induced physical crosslinking. Specifically, the impact of HA concentration on the polymer matrix dispersion, mechanical strength, and biocompatibility was evaluated. Notably, our goal is to determine the optimal concentration of HA that balances mechanical robustness with biological functionality. To achieve this, several tests were conducted to assess the hydrogel's mechanical properties, cellular compatibility, and its potential to support osteogenic differentiation. The incorporation of hydroxyapatite into a chitosan-based hydrogel aims to mimic the natural composition of bone, to fabricate a scaffold that promotes osteoinductivity [44,45] and mimics the native bone extracellular matrix, a viable environment for mesenchymal adipose stem cells. Chitosan-based hydrogels were crosslinked using a NaOH crosslinking agent to obtain pH variation of acidic chitosan solution, thus inducing a physical crosslinking. The physical, chemical, and morphological properties of the hydrogels were investigated. Mechanical and rheological tests were conducted to assess how the filler modified the mechanical and structural stability of the hydrogel. Furthermore, spheroids of adipose-derived stem cells (SASCs) were seeded on these hydrogels to assess their biocompatibility and osteogenic potential. The combination of these materials with a 3D spheroid culture model provides a novel approach to studying osteogenesis. By focusing on SASCs, this research also aims to further the use of adipose tissue as a suitable source of stem cells for BTE. The results highlight the ability of these nanocomposite hydrogels to support cell viability and osteogenic differentiation, underscoring their potential as customizable scaffolds for bone tissue engineering.

2. Materials and methods

2.1. Materials

High molecular weight chitosan (Chi), nano-hydroxyapatite (200 nm, according to the supplier), acetic acid (AA) (for analysis, 99.8 %), sodium hydroxide (NaOH) (ACS reagent, ≥97.0 %, pellets) were purchased from Sigma-Aldrich (St. Louis, MO, USA). Dulbecco's Phosphate-Buffer Saline (PBS pH 7.4) was purchased from Gibco (Carlsbad, CA).

2.2. Preparation of chitosan-based hydrogel

The chitosan polymer solution (2 wt%) was prepared by dissolving it in a 0.5 vol% aqueous acetic acid solution at 40 °C for 5 h under controlled stirring. For the chitosan/HA suspensions, the HA powder was suspended in an aqueous AA solution containing 0.5 % (v/v) of AA with different concentrations (10, 20, and 30 wt% with respect to the chitosan phase) for 15 min in an ultrasonic bath. Then, Chi was added to the suspension and dissolved at $T = 40$ °C for 5 h under a controlled magnetic stirrer. The crosslinking agent was prepared by adding 2 g of NaOH to 50 mL of deionized water to achieve a final concentration equal to 1 M.

To obtain cylindrical scaffolds, the Chi and Chi/HA solutions were loaded into polymethyl methacrylate molds, with a height of 2 mm and different diameters. A paper filter soaked in NaOH was placed under and over the mold in a Petri dish for 5 min. After the filter was removed, the crosslinking procedure was reached by immersing the mold in a NaOH bath for 15 min. Once the crosslinking process was completed, the hydrogels were soaked in deionized water to remove any excess NaOH.

2.3. Morphological characterization

The morphology of chitosan-based hydrogels was observed by scanning electron microscope (SEM) (FEI Quanta 200 F, FEI, USA). Chi and Chi/HA hydrogel samples with diameters equal to 15 mm and 2 mm

height were frozen at −80 °C and freeze-dried (FreeZone Triad by Labconco corporation, USA, Missouri, Kansas City) at −30 °C and 0.220 mbar for 24 h. After water removal, the samples were fractured under liquid nitrogen and attached to an aluminum stub using adhesive carbon tape. Before the analysis, the samples were coated with a thin gold layer using a Sputtering Scancoat Six (Edwards Laboratories, Milpitas, CA, USA) for 60 s under an argon atmosphere to prevent electrostatic discharge. The average pore size of the hydrogels was measured using ImageJ software.

2.4. FT-IR/ATR analysis

A Fourier transform infrared spectrometer in attenuated total reflectance (FTIR-ATR, model IRTracer - 100 spectrophotometer from Shimadzu, Europe, Italy, Milan) was used to investigate the chemical surface properties of the powdered lyophilized hydrogels. The instrument used attenuated total reflectance Fourier transform infrared (ATR - FTIR) with an operating wavelength of 4000–500 cm^{-1}, and a resolution of 4 cm^{-1}. For each material, five samples were tested and the representative spectra were reported.

2.5. Mechanical characterization

Compression tests were performed on a cylindrical sample measuring 40 mm in diameter and 2 mm in height using a universal testing machine (UTM, model 5943, Instron, UK). The UTM was equipped with a 1 kN load cell and with a BioPulse bath. The tests were conducted in PBS at a temperature of 37 °C. Uniaxial tests to determine the compressive strength and the response under cyclic loading were performed on three samples per each condition.

The uniaxial compression test was performed at a strain rate of 1 mm/min reaching up to 50 % strain. The cyclic tests were performed at a compression/unloading speed of 1 mm/min. Cyclic tests applied quasi-static triangular ramps with maximum forces incrementally increasing from 10 N to 100 N, in 10 N steps. In addition, 100 cycles of compression tests reaching a maximum strain of 16 % in all cycles were conducted at a speed of 1 mm/min. Cyclic tests mimic physiological conditions and allow studying material's ability to withstand mechanical compression under cyclic and repeated loading over time. The elastic modulus (E) and compressive strength (s) were determined from the stress-strain curves. The energy dissipated during compression was determined as the area under the stress-strain curve during the cyclic test. For each material, seven samples were tested for each type of mechanical analysis performed. The stress-strain curves presented are representative of the tested samples, while the mechanical parameters derived from these curves are reported as average values with standard deviations.

2.6. Rheological characterization

The rheological characterization of polymeric solutions and the hydrogels was performed using a Discovery Hybrid Rheometer (HR10 by TA Instrument) with a plate-plane parallel equipped with a Peltier cell. The tests were conducted at a temperature of 37 °C to mimic physiological conditions. The sample had a height of 2 mm and a diameter of 6 cm. A frequency sweep test was carried out for both the polymeric solution and the hydrogels in the frequency range of 0.1–100 Hz with 1 % constant strain. The amplitude sweep test was evaluated with an oscillation strain of 0.1–100 % and a constant frequency of 10 Hz was performed only on cross-linked hydrogels. For each material, five samples were tested and the representative curves were reported.

2.7. In vitro swelling test

To study the swelling behavior of hydrogels, the lyophilized samples ($n = 3$) were immersed in 2 mL of deionized water at 37 °C in a biological incubator. The swelling ratio (%) of the hydrogels was evaluated by measuring the absorbed water as a function of time Eq. (1):

$$Swelling\ ratio\ (\%) = \frac{(W_s - W_d)}{W_s} \times 100 \quad (1)$$

where, W_s and W_d are the weights of the swollen and dried hydrogels, respectively.

2.8. In vitro weight loss test

The weight loss of the samples ($n = 3$) was evaluated by immersing hydrogels in phosphate-buffered solution (PBS) (pH = 7.4) at 37 °C in the incubator to imitate physiological conditions. The weight loss (%) was calculated by considering the mass loss at different time points using the following Eq. (2):

$$Weight\ Loss\ (\%) = \frac{(W_0 - W_t)}{W_0} \times 100 \quad (2)$$

where, W_0 and W_t are the weights at initial time and at different time points, respectively.

For each material, five samples were tested and the curves were reported as average values with standard deviations.

2.9. Cells culture

Adipose tissue samples ($n = 10$) were obtained from healthy subjects after obtaining informed consent from patients. Samples were taken from different anatomical parts (breast, abdominal, and thighs) and digested mechanically (30 min or 1 h depending on whether lipoaspirate or tissue in a 37 °C bath under agitation) and enzymatically (collagenase 150 mg/mL, Gibco, Carlsbad, CA, hyaluronidase 20 mg/mL, Sigma, St. Louis, MO). Next, centrifugation at 1200 rpm for 5 min was performed, and the stromal vascular fraction (SVF) was recovered and resuspended in stem cell medium and ultra-low attachment flasks (Corning, NY, USA). After spheroids isolation occurred, they were counted and stained with the vital dye PKH26 (Sigma) which binds to membranes to monitor the viability and the morphology during the culture. Then, the cells were plated on top of chitosan and chitosan hydroxyapatite scaffolds in osteoblastic differentiation condition (Stempro, Gibco, Carlsbad, CA) and maintained in a 37 °C incubator with 5 % CO_2 for 14 days.

2.10. Cell viability analysis

The cell viability of SASCs under all conditions was quantified by the MTS assay (3-(4,5-dimethylthiazole-2-yl)-5-(3-carboxymethoxyphenyl)-2-(4-sulfophenyl)-2Htetrazolium) assay (Promega, Madison, WI). Cells were plated in biological triplicates at a density of 20,000 cells/well in 96-well plates filled with 100 μL/well of culture medium (control) or 50 μL/well of scaffold and 50 μL/well of culture medium. Fresh medium was added every three days until the end of the experiment. In order to observe the results obtained at 14 days of culture, the spectrophotometer (TECAN Spark 10 M, Switzerland, Europe) was used at an absorbance of 490 nm.

2.11. Immunofluorescence staining

In order to characterize the differentiation of SASCs after 14 days cultured in an osteoblastic medium, cells were first fixed in 4 % formaldehyde for 10 min at room temperature. They were subsequently permeabilized with 0.1 % Triton-X100 and exposed to the rabbit osteopontin antibody (Thermofisher Scientific, Massachusetts, USA) overnight at 4 °C. Then, anti-rabbit alexa fluor 568 secondary antibody (Thermofisher Scientific) was used for 2 h at room temperature and the nuclei were stained with Hoechst for 10 min at room temperature. Immunofluorescence analysis was conducted with a confocal

microscope (Leica DM IL LED Fluo, Wetzlar, Germania).

2.12. Luminex investigation

By Luminex plates (PPX-03-MXYMKX2, Thermofisher Scientific), we analyzed the presence of three analytes related with osteoblastic differentiation (BMP-2, BMP-9 and Osteopontin) in the conditioned media (or cell culture supernatants) at 14 days of *in vitro* culture in all scaffold conditions. According to the manufacturer's instructions, for each cytokine analysis, we subtracted the average value of the basal medium used for the differentiation of SASCs to the blank. Next, an average was performed from each duplicate sample and the data were processed as the intensity value in $\log_{10}$.

2.13. Statistical analysis

The data were analyzed statistically using one-way analysis of variance (ANOVA). When appropriate, comparisons between datasets were conducted using the Student's *t*-test. A significance threshold of $p < 0.05$ was applied. ANOVA was utilized to identify significant variations in the values obtained from sample characterization, with $p < 0.05$ indicating statistical significance.

3. Results and discussions

3.1. Rheological and mechanical characterization

Fig. 1 shows the fabricated Chi and Chi/HA hydrogels with a height of 2 mm and a diameter of 6.5 mm. As shown, it is worth noting that the hydrogel maintains its shape even after the removal of the mold. This ability to retain shape suggests remarkable mechanical stability. In addition, a difference in color between Chi and Chi/HA (10, 20, and 30 wt%) can be qualitatively observed. The Chi hydrogel was more transparent, while the presence of nano-hydroxyapatite gave the Chi/HA hydrogel a milky color.

Tests were performed to evaluate the rheological and mechanical response of the biopolymeric solutions and cross-linked hydrogels [42]. The rheological analyses were essential to assess the effect of different HA concentrations on the viscosity of the polymer solutions and to evaluate the effect of the filler on the stiffness of the chitosan-based hydrogels. Frequency sweep tests were conducted to evaluate key rheological properties, including complex viscosity (η*), storage modulus (SM), and loss modulus (LM). Fig. 2A presents the flow curves and complex viscosity as a function of angular frequency (ω) for each polymeric solution. The flow curves exhibit pseudoplastic behavior, with complex viscosity decreasing as the angular frequency increases. Notably, at low frequencies, the flow curve of the Chi solution flattens, indicating a pseudo-Newtonian behavior. In contrast, the addition of HA nanofillers to the Chi/HA solution results in a significant increase in complex viscosity, particularly at low and medium frequencies, with the viscosity rising as the HA concentration increases. At high frequencies, this effect diminishes, and the complex viscosity approaches values similar to those of the Chi solution. The flow curves further highlight the shear-thinning behavior of the polymeric solutions, where complex viscosity decreases as the applied stress increases, consistent with findings by Tang et al. [46]. The shear-thinning effect becomes more pronounced with higher HA concentrations in the Chi/HA solution, suggesting the formation of a semi-3D nanoparticle network within the chitosan-based suspensions [47]. Fig. 2B shows the storage (SM) and loss modulus (LM) as a function of angular frequency for the polymeric solutions. At high frequencies, the solutions exhibit a liquid-like behavior, with the loss modulus (LM) exceeding the storage modulus (SM) for all formulations. The introduction of HA significantly altered the rheological behavior of the solutions, especially at low frequencies. Specifically, the addition of HA resulted in a marked increase in the storage modulus, which became almost independent of frequency in the nanocomposite solutions. This suggests a transition from liquid-like to solid-like viscoelastic behavior, with the storage modulus increasing in proportion to HA concentration. Notably, the Chi/HA 30 wt% solution exhibits a crossover between the loss and storage moduli [46,48]. This behavior observed at low frequencies can be attributed to the formation of a semi-3D nanoparticle network, which restricts the polymer relaxation process [49]. These findings are consistent with previous research by Adhikari et al. [50] which reported a transition from liquid-like to solid-like response in the low frequency region for a dispersion of hydroxyapatite in an alginate-based bioink.

Fig. 3 shows the results obtained from the frequency sweep test conducted on the hydrogel, confirming a solid-like behavior, characterized by a flat curve of the storage modulus and values of SM much higher than LM as a function of frequency [51]. This solid-like behavior was observed over the frequency range investigated for each hydrogel, confirming the efficacy of the cross-linking protocol. Moreover, the hydrogel exhibited relatively stable G′ and G″ moduli throughout the frequency range, slightly increasing with HA concentration. Chitosan exhibits a soft consistency and ductile properties; however, rheological tests suggest that the incorporation of HA into the chitosan matrix significantly enhances the material's stiffness [52].

To identify the linear viscoelastic region (LVR), the stress range in which G′ is independent of the applied shear stress, an oscillation amplitude sweep test was conducted for each hydrogel. Specifically, the hydrogels were subjected to a stress sweep to the point of rupture.

Fig. 4 illustrates that the G′ values are lower than the G″ values, indicating that all hydrogels exhibit predominantly elastic (solid-like) behavior. Both G′ and G″ increase with higher HA concentrations, suggesting good interfacial compatibility between the polymer matrix and the nanofiller. The cross-over point, where G′ surpasses G″, marks the transition to liquid-like behavior and signifies the disruption of entanglements formed by hydrogen bonds between the deprotonated -NH_2 and -OH groups. This disruption signals the end of the elastic region, occurring at a critical stress [52]. As HA concentration increases, the cross-over point shifts to higher strains, demonstrating that the addition of HA nanoparticles enhances the polymer matrix's resistance to shear stress [52,53]. The liquid-like behavior observed at high frequencies in the Chi/HA 10 wt%, Chi/HA 20 wt%, and Chi/HA 30 wt% formulations can be attributed to the disruption of the nanoparticles' three-dimensional structure [54]. The rheological results highlight the effect of HA concentration on both viscosity and mechanical properties of the chitosan-based hydrogels. These findings confirm that HA acts as a mechanical reinforcement for the hydrogel structure, which are typically characterized by low rigidity.

The mechanical properties of chitosan hydrogels with different HA filler concentrations were assessed through uniaxial compression tests. Fig. 5 presents the stress-strain curves, while Table 1 reports Young's modulus, maximum compression strain, and compressive toughness at 80 % strain. As shown in Fig. 5, the slope of the stress-strain curves increases with higher HA concentrations, indicating increased stiffness. Table 1 shows a rise in Young's modulus from 26.8 kPa for Chi to 63.8 kPa for Chi/HA 30 wt%. The compression strength also increased with

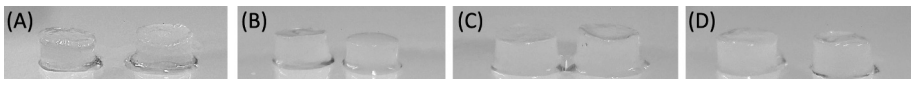

Fig. 1. Comparison of chitosan-based hydrogels (Chi) and chitosan/hydroxyapatite (Chi/HA) nanocomposite hydrogels containing 10 wt%, 20 wt%, and 30 wt% HA. The images highlight differences in color and transparency, indicating HA incorporation.

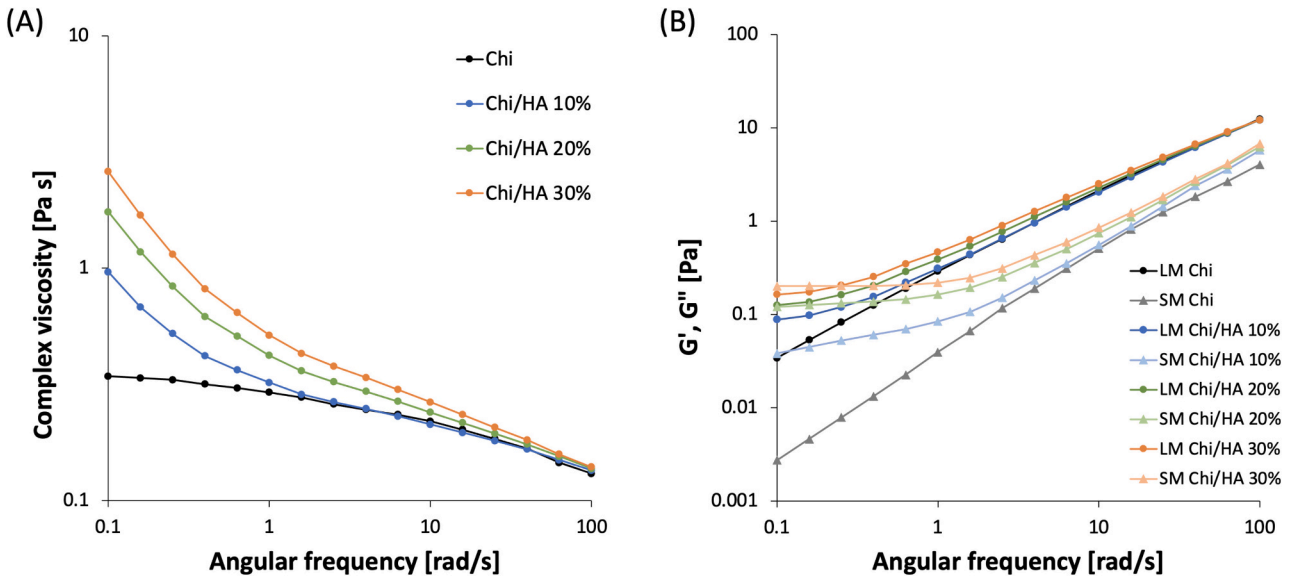

Fig. 2. Rheological behavior of polymeric solutions: (A) Representative flow curves showing complex viscosity *versus* angular frequency, demonstrating shear-thinning behavior with increasing HA concentration; (B) representative storage modulus (SM) and loss modulus (LM) as a function of angular frequency, revealing HA's impact on viscoelastic properties. For each material, the curves shown represent one of the five tested samples.

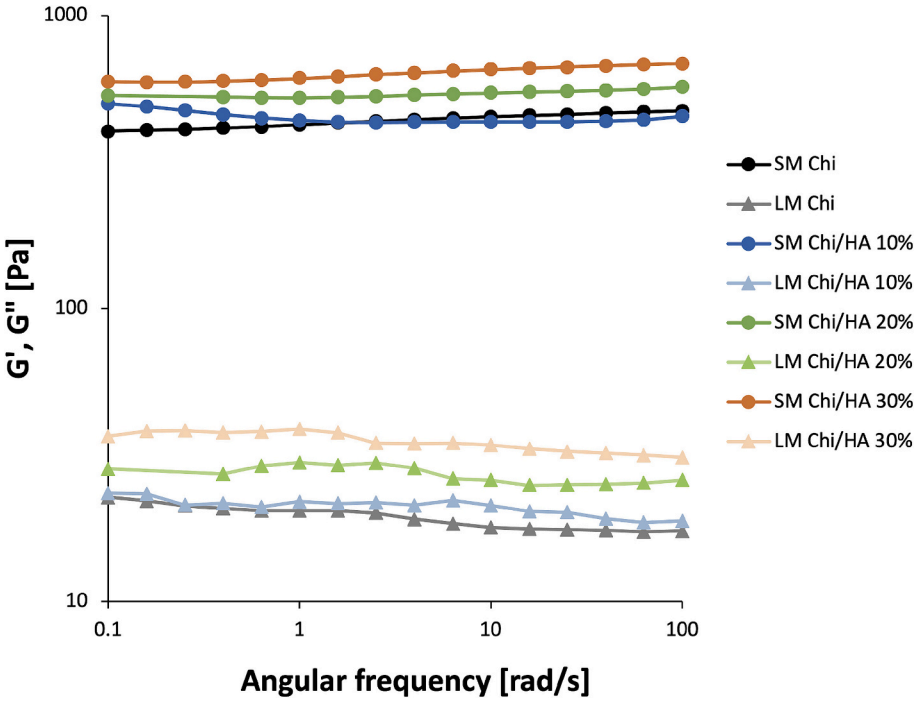

Fig. 3. Rheological properties of hydrogels. Representative storage (SM) and loss modulus (LM) as a function of angular frequency confirm the solid-like behavior of Chi and Chi/HA hydrogels and the stiffening effect of HA. For each material, the curves shown represent one of the five tested samples.

HA: 70 kPa for Chi, 90 kPa for Chi/HA 10 wt%, 140 kPa for Chi/HA 20 wt%, and 183 kPa for Chi/HA 30 wt%.

Compressive toughness rose from 1309.26 kJ/m^3 for Chi to 3657.57 kJ/m^3 for Chi/HA 30 wt%. Different factors such as HA particle size and distribution, mechanical properties of the chitosan, and interfacial interactions between chitosan and HA can contribute to changing the mechanical properties of the material [55]. The results suggest that the addition of HA nanofiller, acting as a mechanical reinforcement, effectively improved the mechanical strength of the hydrogel structure, as confirmed in the literature [56,57]. This may be due to good interaction between HA and the Chi matrix and to the formation of secondary crosslinking points between Chi and HA, able to reduce the free movement of polymer chains [58], coherently with the morphological results that will be discussed later.

For application as bone-tissue materials, hydrogels are required to bear repetitive loads for a short time; therefore, a fatigue cycle test was conducted to assess the performance of the hydrogels.

Cyclic compression tests were performed to evaluate the hydrogel's performance under repeated stress (Fig. 6). Panels A to D of Fig. 6 show the stress-strain curves for Chi and Chi/HA composites (10 wt%, 20 wt %, and 30 wt%) up to 100 cycles. Hysteresis decreased in subsequent cycles, stabilizing, which indicates rapid self-recovery and fatigue

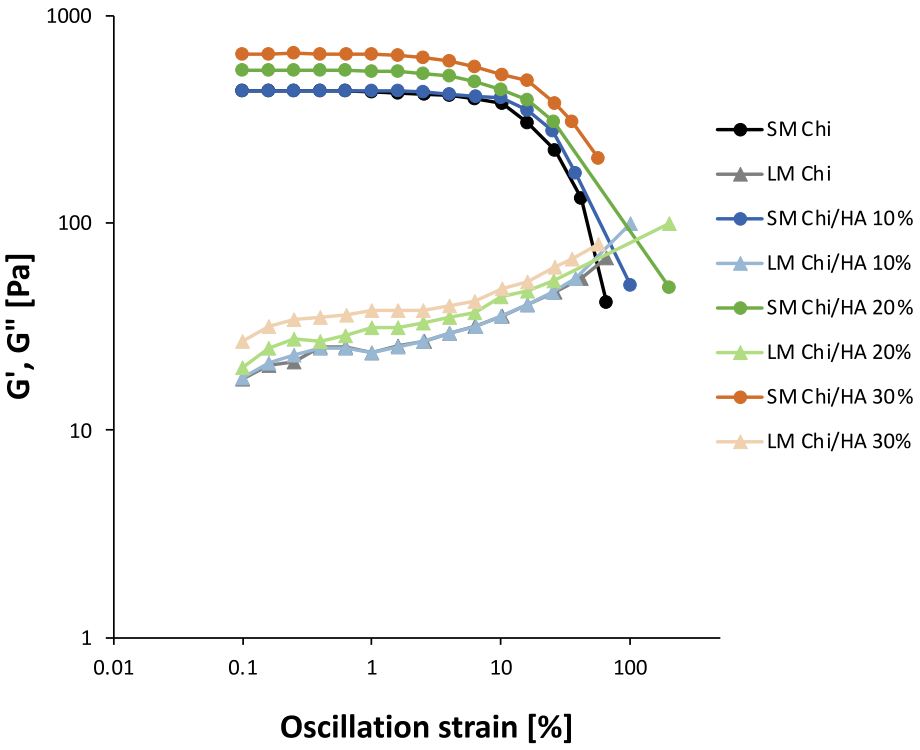

Fig. 4. Representative oscillation strain sweep test results for hydrogels. Storage modulus (SM) and loss modulus (LM) indicate enhanced elasticity and resistance to deformation with higher HA concentrations. For each material, the curves shown represent one of the five tested samples.

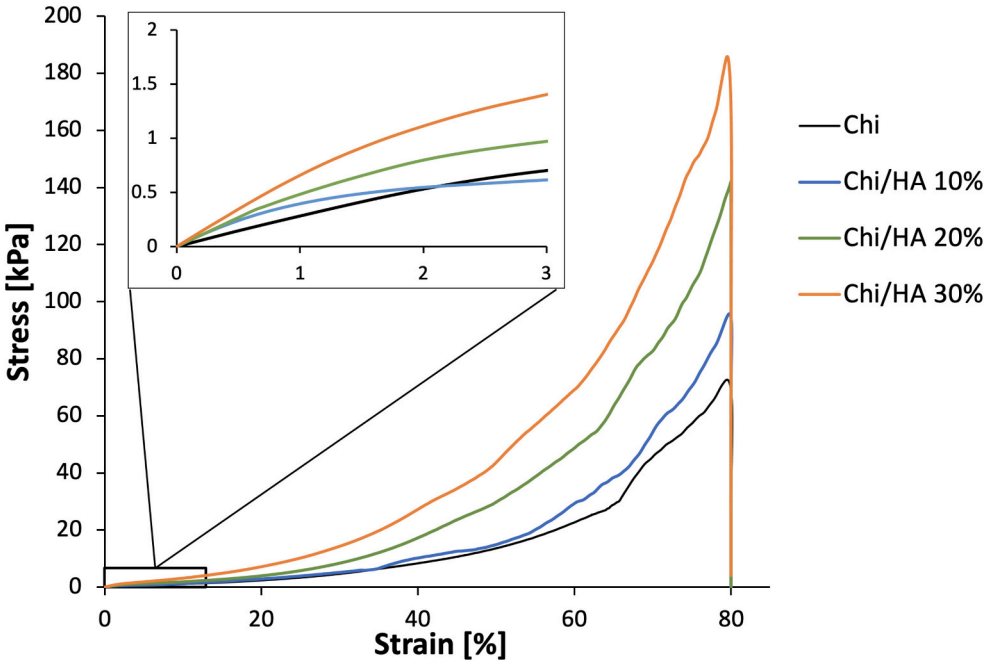

Fig. 5. Representative stress-strain curves from uniaxial compression tests of Chi and Chi/HA hydrogels. Increasing HA concentration improves stiffness and mechanical strength. For each material, the curves shown represent one of the seven tested samples.

resistance. In the first cycle, a larger hysteresis was observed, likely due to the breaking of chemical crosslinks [52]. As the cycles progressed, hysteresis decreased and stabilized, indicating that the hydrogels exhibit rapid self-recovery and fatigue resistance [52]. This behavior suggests that the hydrogels are able to reorganize and dissipate energy effectively during deformation, consistent with previous reports [3,60].

Additionally, Fig. 7 quantifies the dissipated energy for each cycle, which was influenced by both HA concentration and the number of cycles. Higher HA concentrations and more cycles resulted in a more elastic material, showing improved recovery and resilience. The tighter hysteresis and enhanced energy dissipation observed in the samples highlight the significant impact of HA concentration and cyclic loading on the hydrogel's mechanical performance [52,61]. The mechanical testing clearly demonstrated a significant increase in both Young's

Table 1
Summary of mechanical properties of Chi and Chi/HA hydrogels. Increasing HA concentrations enhance Young's modulus, compressive strength, and toughness. Significant differences within the same column ($p < 0.05$) are indicated by different letters, as determined using multiple Student's *t*-tests.

Sample	Elastic modulus E [kPa]	Compressive strength [kPa]	Compressive toughness [kJ/m^3]
Chi	26.8 ± 1.01^a	70 ± 1.32^a	1309.26 ± 2.32^a
Chi/HA 10 %	30.3 ± 5.78^b	90 ± 5.45^b	1591.36 ± 3.57^b
Chi/HA 20 %	40.8 ± 6.14^c	140 ± 6.12^c	2566.19 ± 2.57^c
Chi/HA 30 %	63.8 ± 6.3^d	183 ± 6.78^d	3657.57 ± 4.71^d

modulus and compressive strength correlated with HA concentration. This enhancement in mechanical stability is crucial for the fabrication of materials capable of providing the necessary structural support. Furthermore, the composite hydrogel exhibits promising mechanical properties for bone tissue applications, demonstrating rapid self-recovery and resistance to cyclic loading forces. These results are consistent with the findings of Kumar et al. [52], which demonstrated the ability of HA to enhance the Young's modulus of a Chi-based hydrogel, even though the filler concentrations used in their study were an order of magnitude lower.

3.2. Morphological analysis

Fig. 8 shows the morphology of the cross-sectioned lyophilized hydrogels. As can be observed, the freeze-drying process resulted in an interconnected and defined porous structure with an average pore diameter of ~ 200 μm in the case of Chi hydrogel and ~ 100 μm in the case of Chi/HA hydrogel, also featured by very thin walls, in agreement with scientific literature [52,37,63]. As already observed in other works [22], the addition of HA led to a reduction of the mean pore size of the structure. According to Emami et al. [65] this result can be ascribed to an increase in the crosslink density in the presence of HA nanoparticles that can act as secondary crosslinking points for Chi, resulting in a more compact architecture. At higher magnification, the presence of HA nanoparticles can be observed in the Chi/HA samples. As expected, the number of particles increases upon increasing the HA concentration in the hydrogel.

The SEM analysis shows that the nanoparticles are homogeneously distributed in the polymer matrix and their average diameter is almost uniform, confirming that the nanoparticles are well-dispersed in the polymer solution. This indicates an efficient dispersion process, ensuring that the nanoparticles are adequately integrated into the polymer solution. The proper distribution of the nanoparticles is crucial for improve the material's properties.

3.3. FTIR-ATR analysis

The chemical features of HA particles, and lyophilized Chi and Chi/HA hydrogels were evaluated using FTIR-ATR spectroscopy (Fig. 9). The spectra of nano HA particles showed a strong absorption band around 1021 cm^{-1} corresponding to the asymmetric stretching vibration mode of phosphate PO_4 bend (ν_3), and PO_4 stretch (ν_3) at 962 cm^{-1} [66–68]. The peaks at 601 cm^{-1} and 565 cm^{-1} are attributed to the stretching of P—O bonds or the ν_4 phosphate mode vibrations [66,67]. The bands at 875 cm^{-1} and 1450 cm^{-1} correspond to the ν_2 vibration and the stretching vibrations of the carbonate group (CO_3^{2-}), respectively [69]. The FTIR spectra of Chitosan show a peak at 1550 cm^{-1} corresponding to C—N bending and a peak at 1150 cm^{-1} and 1090 cm^{-1} describing the C—O stretching [70]. It is possible to see that the absorption band around 1600 and 1650 cm^{-1} corresponds to the stretching of C═O [70]. The other characteristic peaks of Chitosan at 3450 cm^{-1}, 3300 cm^{-1}, and 2900 cm^{-1} correspond to the stretching of bond O—H, amine I, and C—H, respectively [70], not shown in Fig. 9. Chi/HA composites showed

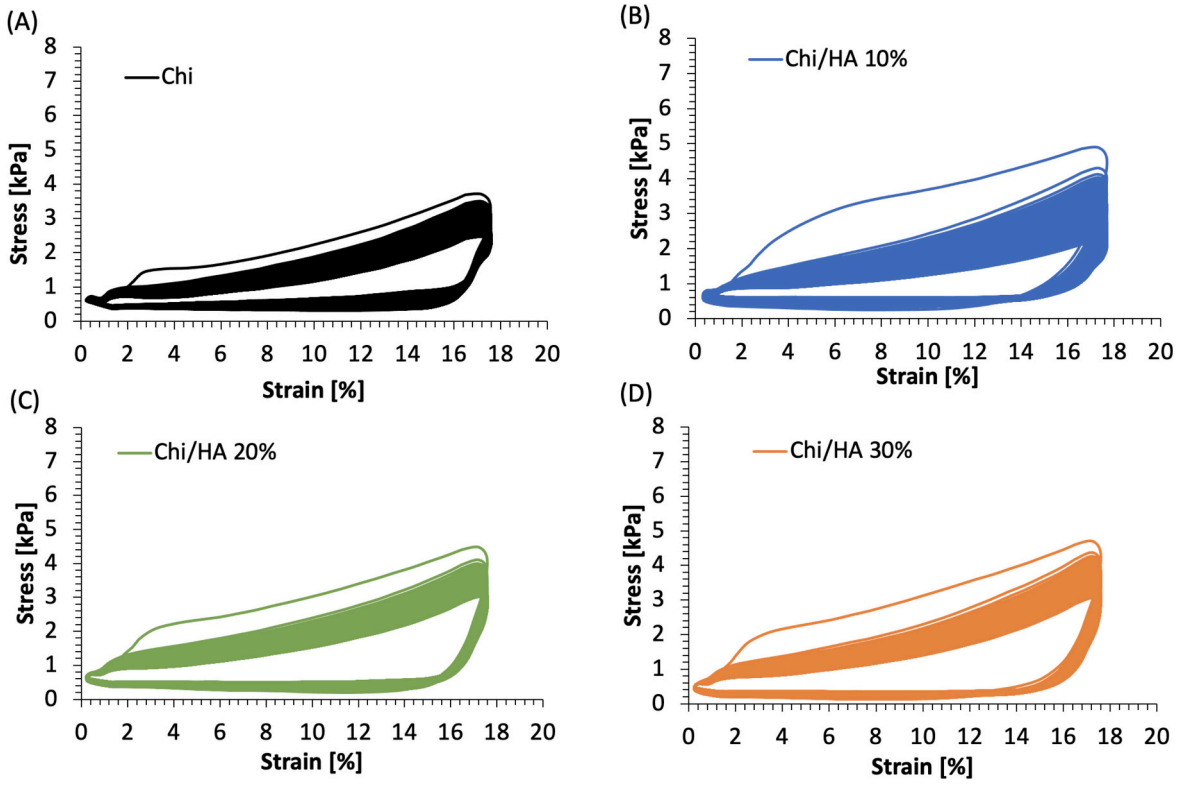

Fig. 6. Cyclic compression behavior of hydrogels. Stress-strain curves for Chi and Chi/HA hydrogels after 100 cycles show rapid recovery and fatigue resistance. For each material, the curves shown represent one of the seven tested samples.

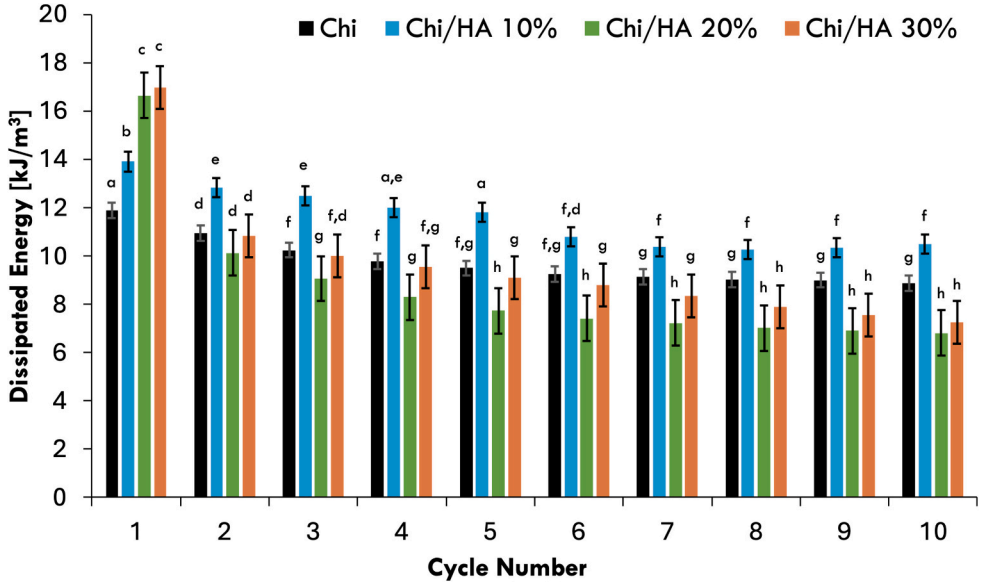

Fig. 7. Dissipated energy during cyclic compression. Hydrogels with higher HA concentrations exhibit increased elasticity and reduced energy loss, demonstrating better structural recovery. Significant differences ($p < 0.05$) are indicated by different letters, as determined using multiple Student's *t*-tests.

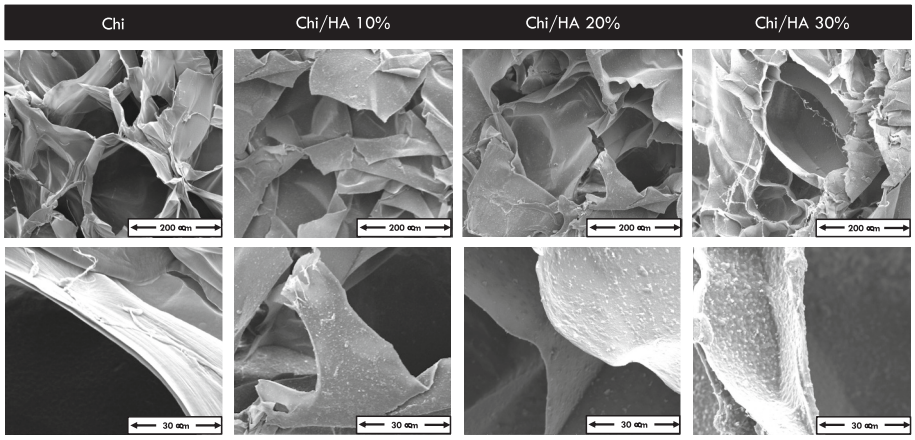

Fig. 8. SEM images of Chi and Chi/HA hydrogels. The porous structures of hydrogels are shown, with smaller pore sizes observed as HA concentration increases.

the characteristic peaks of both, chitosan and HA samples, although the peaks related to HA particles were overlapped by the more intense peaks of chitosan. The PO_4 peak at 601 cm^{-1} and 560 cm^{-1} can also be easily recognized in the composite hydrogels and did not show any wavelength shifts compared to the nanohydroxyapatite. As expected, results showed that the intensity of the peaks ascribable to the HA particles increased with increasing filler concentration in the composites [52,71]. It is noticeable that with the addition of HA, the intense peak at about 1021 cm^{-1} becomes more prominent, overlapping with the chitosan peak at 1090 cm^{-1}, which appears less distinct. This phenomenon was more prominent as the concentration of HA in the composites increased. The absence of wavelength shifts in the Chi/HA composites suggested that the interactions between the two phases were only physical without any chemical reaction. The results effectively confirm the presence of HA in the hydrogel structure, indicating a successful dispersion process.

3.4. Loss weight test

The evaluation of weight loss of hydrogel is an important factor to evaluate its stability in a physiological environment and its applicability. Typically, the degradation of the polymer occurs due to processes such as simple dissolution, hydrolysis, and enzymatic activity. The hydrolytic process involves the cleavage of covalent bonds with water [72]. The weight loss analysis for each formulation was carried out *in vitro* at 37 °C in PBS, as presented in Fig. 10. All samples have proven to gradually lose weight during the 21 days of incubation. The samples containing the higher HA concentration (Chi/HA 30 wt%) experienced lower weight loss. This can be attributed to the stabilizing effect of HA, which, through its phosphate groups, helps to buffer the degradation process. This finding is consistent with previous studies, including those by Triyono et al. [73], who observed a similar effect in HA-incorporated nanocomposite hydrogels. In addition, B. Kaczmarek et al. [74] also reported that the incorporation of HA in composite materials contributes to a reduction in degradation rates. This further supports the notion that HA plays a critical role in enhancing the material's stability under physiological conditions, possibly by influencing both the physical and chemical degradation pathways.

3.5. Swelling test

Fig. 11 shows the swelling ratio of Chi and Chi/HA hydrogels at 0, 15, and 30 min, 1, 5, and 24 h. The results suggest that the Chi sample tends to swell slightly more than the others. Nonetheless, all hydrogels achieved equilibrium after 15 min of immersion in water. The addition

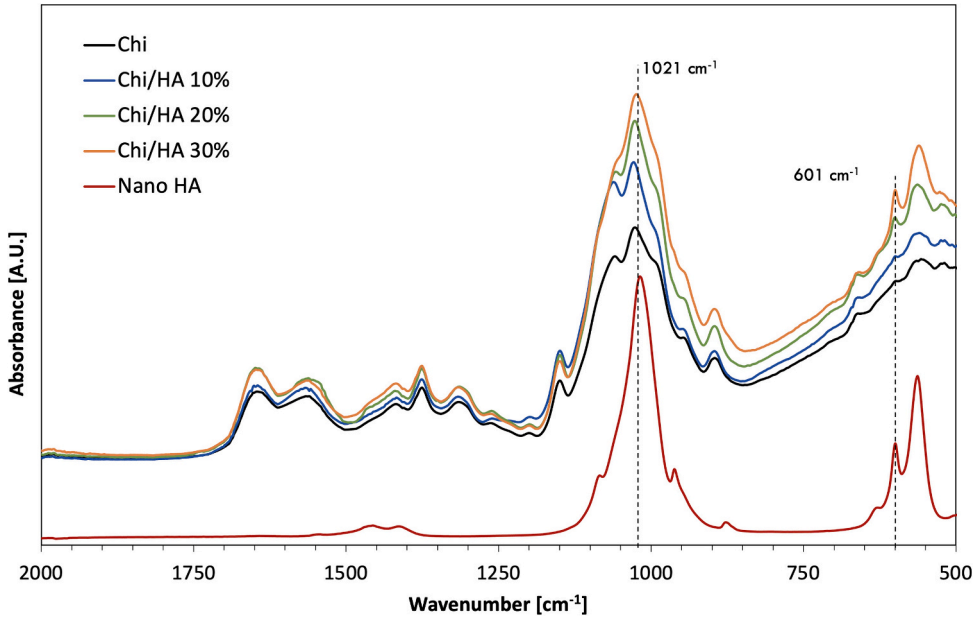

Fig. 9. FTIR-ATR spectra of nanohydroxyapatite (HA), Chi, and Chi/HA hydrogels. Characteristic peaks indicate the successful incorporation of HA without chemical interactions. For each material, the spectra show one of the five tested samples.

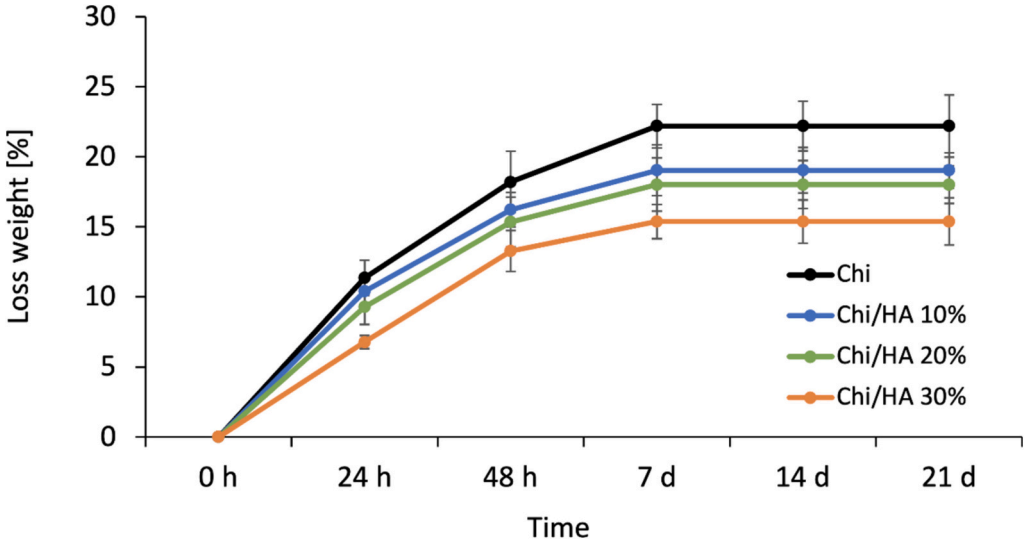

Fig. 10. Weight loss of hydrogels over 21 days in PBS. Hydrogels with higher HA concentrations demonstrate improved stability and reduced degradation. Data reported as average values of five samples with standard deviations.

of HA slightly changed the swelling characteristics, specifically by decreasing it [75]. The statistical analysis revealed a significant difference only between the Chi sample and the Chi/HA nanocomposite systems, indicating an 'on-off' effect attributed to the additive. However, this effect appears independent of the additive's concentration in the hydrogel system. This behavior can be likely explained by assuming that HA acts as a physical impediment to the absorption of water by the lyophilized structure. This could be due to the reinforcement created by the additional hydrogen bonds which hinder the free movement of the polymer chain [75,57]. In addition, the reduced swelling ratio may also be correlated to the pore structure of the hydrogels. As highlighted in the scientific literature, a smaller average pore size is associated with lower swelling capacity, as smaller pores limit the space available for water retention [75,77]. This phenomenon aligns with previous findings, which reported that larger pores facilitated greater water uptake and consequently enhanced swelling behavior [74,78]. The presence of HA in the hydrogel matrix likely influences the pore morphology, resulting in a denser and more compact network. This structural modification might explain the observed changes in the swelling behavior, further supporting the hypothesis of HA acting as a structural and functional modifier of the hydrogel matrix [52].

3.6. Biological analysis

The viability of SASCs was quantified by MTS analysis on the cell-seeded onto scaffolds at 14 days when osteoblastic differentiation is expected to have already happened. Analyses showed an increase of proliferation into Chi (1.5 fold) and Chi/HA 10 wt% (2 fold) when compared with the culture condition without the scaffold. A different behavior was observed when the concentration of HA increased. In fact, SASCs showed a preserved viability into Chi/HA 20 wt% and a slight decrease into Chi/HA 30 wt% (Fig. 12A). This behavior is likely

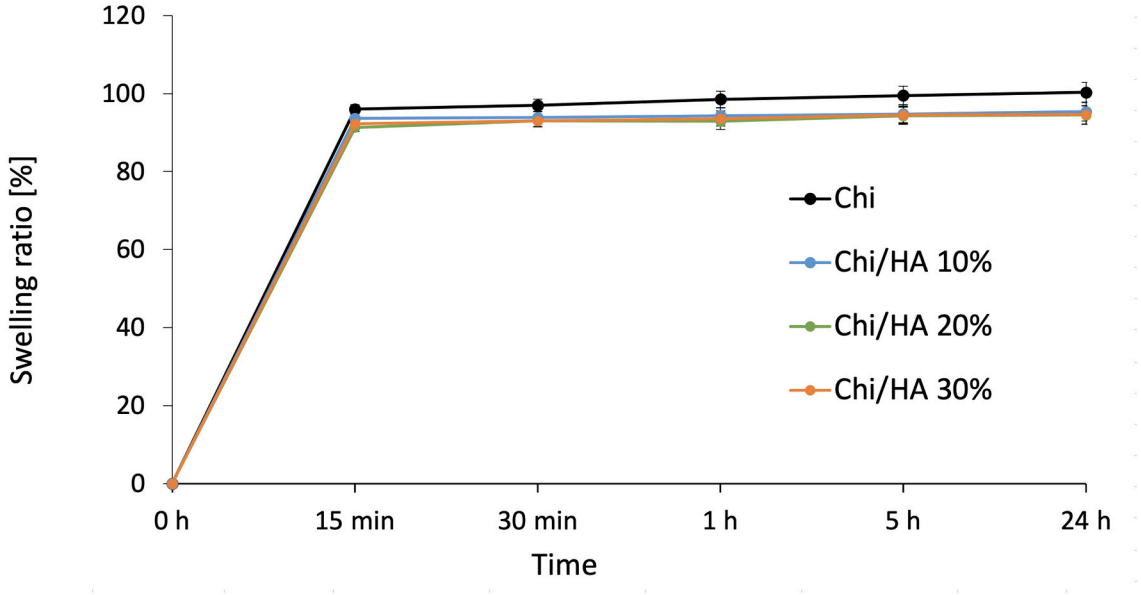

Fig. 11. Swelling behavior of hydrogels. Swelling ratios decrease with increasing HA concentration, suggesting HA's impact on water absorption. Data reported as average values of three samples with standard deviations.

associated with the osteoinductive properties of HA, which promote a shift from cell proliferation to differentiation. This hypothesis is also confirmed by a study by Soriente et al., where they observe the viability of mesenchymal stem cells in osteoinductive medium cultured on Chi and HA at 50, 60 and 70 %, reporting a reduction in viability at high concentrations [79]. In addition, scaffold porosity and pore size play a predominant role in seeding, cell proliferation, nutrient and oxygen diffusion, and overall true tissue formation [80]. In this context, it has been observed that HA scaffolds with higher porosity allow vascularization, providing sufficient oxygen and nutrient flow to allow direct bone formation in *in vivo* rat models compared with those with lower porosity [81]. These results allow us to state that conditions in which there is a high concentration of hydroxyapatite lead to a decrease in the porosity of the scaffold, with consequent stress on the cells, as observed in this study. To track whether the scaffold can support the proliferation and osteoblastic differentiation of SASCs, they were labeled with the red PKH26 dye, which stains the cell membrane of living cells, and placed within the different scaffolds with osteoblast differentiation medium. The morphology of the cells in the systems was examined through fluorescence microscopy, showing a cell distribution on the surface and in the layer thickness of the scaffold after 14 days of culture (Fig. 12B/C/D/E).

In addition, to validate the successful differentiation into osteoblastic cells, we evaluated the osteopontin expression, a typical protein that plays a role in bone homeostasis by providing the basis on which bone forms [57,82] and the production of osteoblastic markers (BMP-2, BMP-9 and osteopontin) in the conditioned medium of the samples. The confocal microscopy z-stack visualization confirmed the presence of osteopontin-positive cells in all systems, as can be seen in Fig. 13. Furthermore, the quantification of the Z size showed the effective colonization of the cells seeded on the top of the systems, with the range of 25–200 μm. Surprisingly, instead, BMP-2 was released in small quantities (10 pg/mL) in all samples, BMP-9 wasn't express and osteopontin only in the control group: SASCs. A possible interpretation of these data is that these factors didn't release in the medium but they were perhaps deposited on the scaffold. In particular, the osteopontin expression was found in intracellular space, as visible in Fig. 13 [83,84].

4. Conclusion

In this work, nanocomposite chitosan-based hydrogels for bone tissue engineering applications were successfully produced *via* pH-induced cross-linking. The effect of the nanometric hydroxyapatite concentration, from 10 wt% to 30 wt%, on the chemical-physical properties of the hydrogels was systematically investigated. Rheological analysis highlighted the ability of the nanometric filler to induce a shear-thinning behavior on the chitosan solutions as well as the efficacy of the cross-linking protocol. Mechanical tests demonstrated that the hydrogel's stiffness could be adjusted by varying the HA concentration, exhibiting an increase of the elastic modulus higher than 100 % when 30 wt% of HA is loaded in the hydrogel. The nanocomposite hydrogels showed rapid self-recovery and resistance to cyclic loading applications, as confirmed by compressive fatigue tests up to 100 cycles. The weight loss analysis revealed that HA improves the *in vitro* stability of the hydrogel by reducing the weight-loss ratio and the total weight loss up to 21 days. The swelling capacity of the hydrogels was minimally influenced by HA incorporation and remained consistent across different HA concentrations. Biological evaluation conducted by seeding mesenchymal stem cells derived from adipose tissue (SASCs) shows the scaffolds' biocompatibility and the HA effect in osteoinductivity behavior. The findings suggest that the chitosan-based hydrogel incorporating 10 wt% HA concentration provides a promising scaffold for bone tissue engineering. Despite the promising results, some limitations should be noted. This study focused on short-term properties, neglecting the long-term stability and degradation behavior, which are crucial for clinical applications. Biocompatibility and osteogenic differentiation were conducted *in vitro*, which may not fully replicate the *in vivo* microenvironment. Additionally, only three concentrations of HA (10 %, 20 %, and 30 %) were tested, suggesting that a wider range of concentrations could provide a more comprehensive understanding. Biocompatibility was assessed using a single 3D cell model (SASCs), but evaluating multiple cell lines or co-culture systems would provide a comprehensive insight into the hydrogel's performance. Future studies should explore the incorporation of cells within the polymer matrix to create a cell-laden structure or a bioink, as well as investigate regenerative properties of these materials in dynamic culture systems such as Organ-on-Chip models or bioreactors, which more closely mimic the physiological environment. Additionally, *in vivo* studies should be conducted to

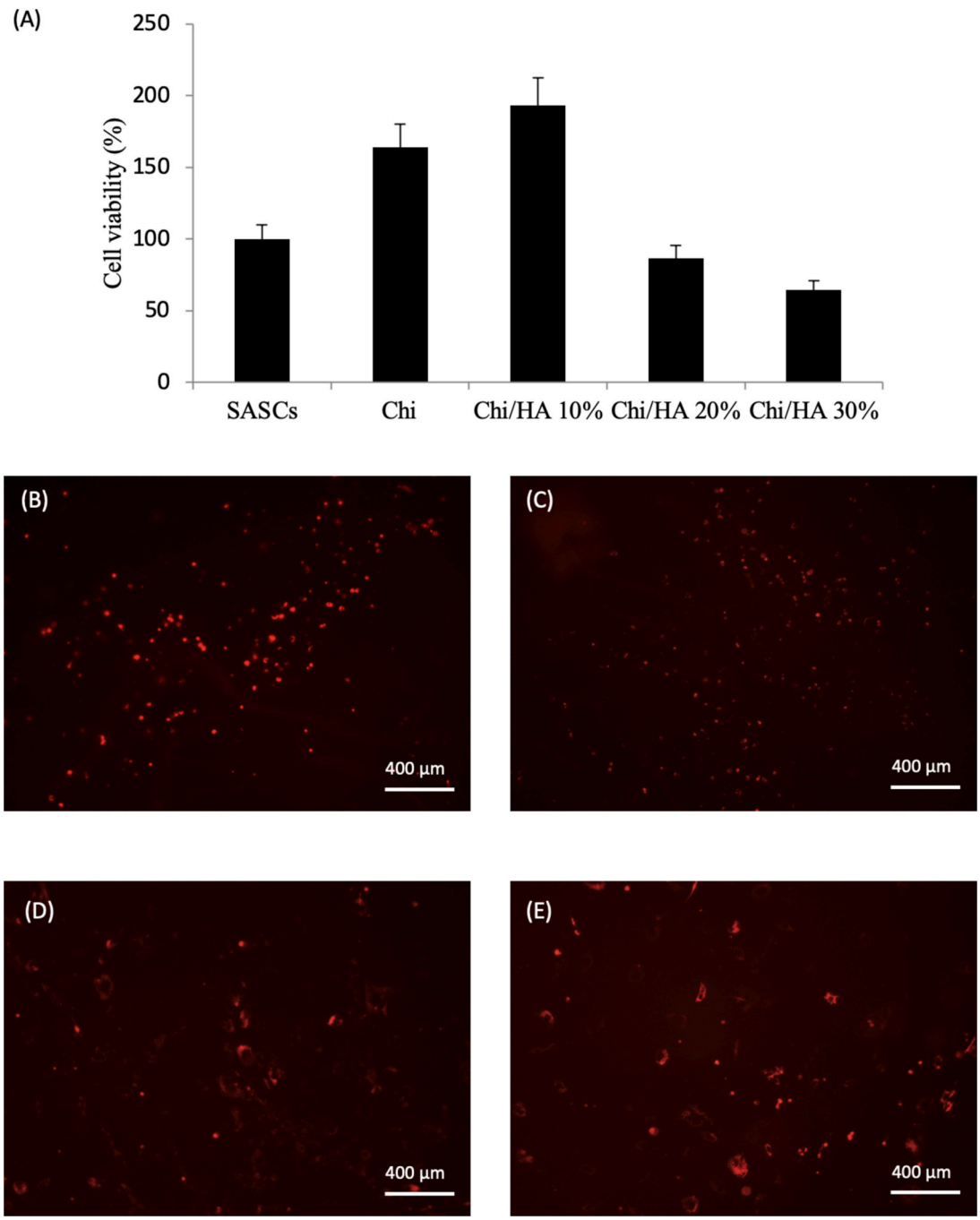

Fig. 12. Cell viability of SASCs (A) and fluorescence PKH26^{+} viable cells respectively in Chi (B), Chi/HA 10 wt% (C), Chi/HA 20 wt% (D), and Chi/HA 30 wt% (E) after 14 days of *in vitro* culture. Data reported as average values of three samples with standard deviations.

evaluate the performance of the most promising scaffolds under physiological conditions. These approaches could provide valuable insights into the scaffolds' potential for clinical translation. The use of primary cells, as demonstrated in this work, underscores the relevance of these materials in the field of personalized medicine, paving the way for tailored bone regeneration strategies.

CRediT authorship contribution statement

A.B. Di Stefano: Writing – original draft, Visualization, Supervision, Methodology, Investigation, Formal analysis, Conceptualization. **C. Di Marco:** Writing – original draft, Visualization, Investigation, Formal analysis. **F. Toia:** Writing – review & editing, Conceptualization. **M. Trapani:** Writing – original draft, Visualization, Investigation, Formal analysis. **M. Testa:** Investigation, Formal analysis. **S. Di Leonardo:** Writing – original draft, Resources, Formal analysis. **G. Burriesci:** Writing – original draft, Resources, Formal analysis. **M. Franza:** Resources, Formal analysis. **E. Cammarata:** Resources, Formal analysis. **A. Cordova:** Writing – review & editing, Conceptualization. **F. Lopresti:** Writing – original draft, Supervision, Methodology, Investigation, Formal analysis, Conceptualization. **V. La Carrubba:** Supervision, Conceptualization.

Funding

Francesco Lopresti is funded by the European Social Fund (ESF)

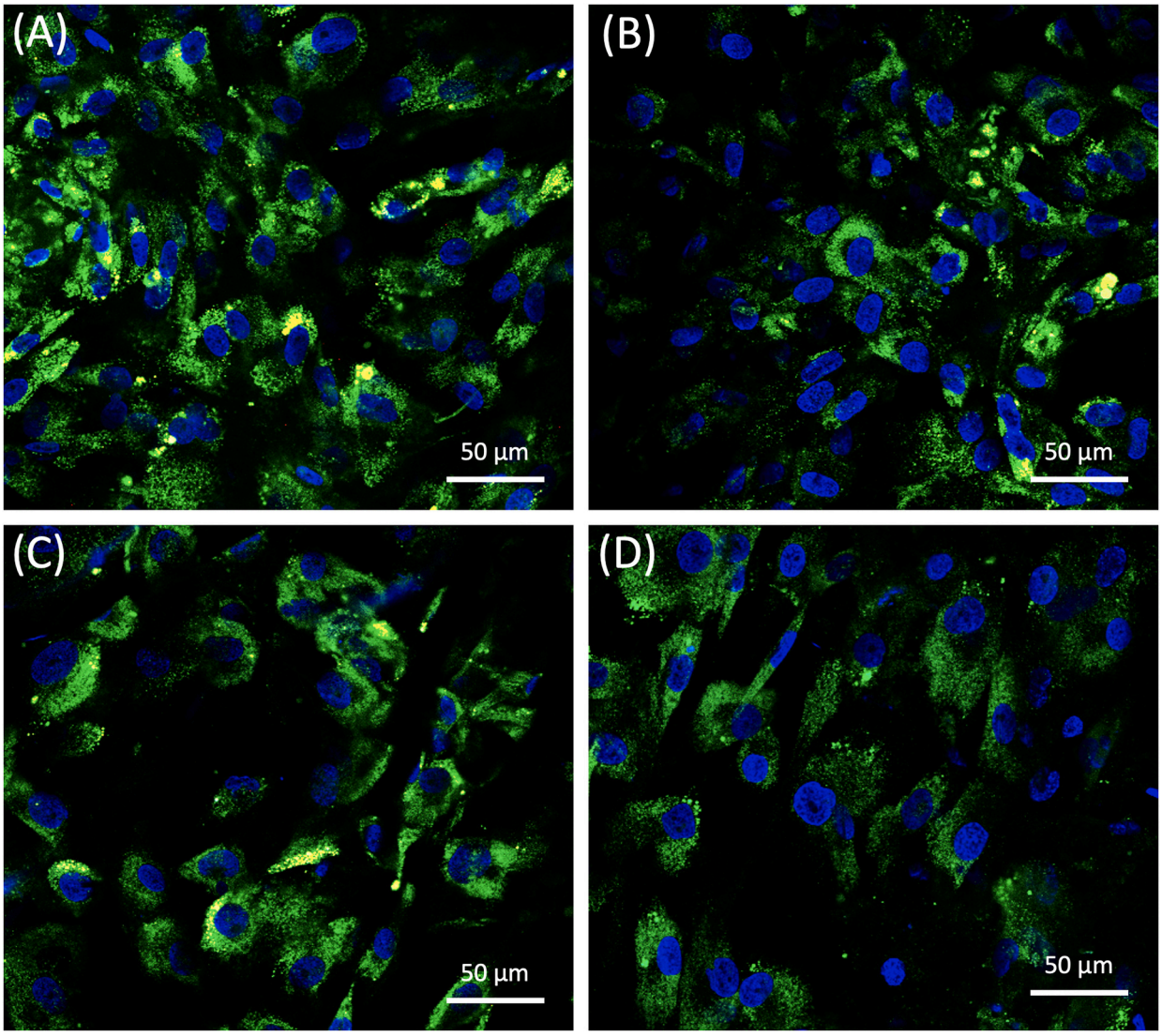

Fig. 13. Representative immunofluorescence z-stack image of Osteopontin (green) and Hoechst (blue) respectively in Chi (A), Chi/HA 10 wt% (B), Chi/HA 20 wt% (C), and Chi/HA 30 wt% (D) after 14 days of *in vitro* culture. (For interpretation of the references to color in this figure legend, the reader is referred to the web version of this article.)

[PON A.I.M: Attraction and International Mobility AIM1845825 – 1. CUP: B74I18000260001].

Declaration of competing interest

The authors declare that they have no known competing financial interests or personal relationships that could have appeared to influence the work reported in this paper.

Data availability

The data presented in this study are available on request from the corresponding author.

References

[1] A. Salhotra, H.N. Shah, B. Levi, M.T. Longaker, Mechanisms of bone development and repair, Nat. Res. Forum (Nov. 01, 2020), https://doi.org/10.1038/s41580-020-00279-w.

[2] R. Agarwal, A.J. García, Biomaterial Strategies for Engineering Implants for Enhanced Osseointegration and Bone Repair, Elsevier B.V., Nov. 01, 2015, https://doi.org/10.1016/j.addr.2015.03.013.

[3] C. Xiang, et al., A porous hydrogel with high mechanical strength and biocompatibility for bone tissue engineering, J Funct Biomater 13 (3) (Sep. 2022), https://doi.org/10.3390/jfb13030140.

[4] F. Schulze, A. Lang, J. Schoon, G.I. Wassilew, J. Reichert, Scaffold Guided Bone Regeneration for the Treatment of Large Segmental Defects in Long Bones, MDPI, Feb. 01, 2023, https://doi.org/10.3390/biomedicines11020325.

[5] V. Šromová, D. Sobola, P. Kaspar, A Brief Review of Bone Cell Function and Importance, Multidisciplinary Digital Publishing Institute (MDPI), Nov. 01, 2023, https://doi.org/10.3390/cells12212576.

[6] L. Suamte, A. Tirkey, J. Barman, P.J. Babu, Various manufacturing methods and ideal properties of scaffolds for tissue engineering applications, Smart Materials in Manufacturing 1 (2023) 100011.

[7] S. Midha, et al., Tissue-specific mesenchymal stem cell-dependent osteogenesis in highly porous chitosan-based bone analogs, Stem Cells Transl. Med. 10 (2) (Feb. 2021) 303–319, https://doi.org/10.1002/sctm.19-0385.

[8] W. Mende, R. Götzl, Y. Kubo, T. Pufe, T. Ruhl, and J. P. Beier, "The Role of Adipose Stem Cells in Bone Regeneration and Bone Tissue Engineering," May 01, 2021, MDPI. doi: https://doi.org/10.3390/cells10050975.

[9] C. McKee and G. R. Chaudhry, "Advances and Challenges in Stem Cell Culture," Nov. 01, 2017, Elsevier B.V. doi: https://doi.org/10.1016/j.colsurfb.2017.07.051.

[10] G. Storti, M. G. Scioli, B. S. Kim, A. Orlandi, V. Cervelli, and F. De Francesco, "Adipose-derived Stem Cells in Bone Tissue Engineering: Useful Tools With New Applications," 2019, Hindawi Limited. doi: https://doi.org/10.1155/2019/3673857.

[11] C. I. Codrea et al., "Clinical medicine advances in osteoporotic bone tissue engineering," J. Clin. Med, p. 10, 2021, doi: https://doi.org/10.3390/jcm.

[12] P.R. Baraniak, T.C. McDevitt, Scaffold-free culture of mesenchymal stem cell spheroids in suspension preserves multilineage potential, Cell Tissue Res. 347 (3) (2012) 701–711, https://doi.org/10.1007/s00441-011-1215-5.
[13] Y. Yamaguchi, J. Ohno, A. Sato, H. Kido, T. Fukushima, Mesenchymal stem cell spheroids exhibit enhanced in-vitro and in-vivo osteoregenerative potential, BMC Biotechnol. 14 (1) (Dec. 2014), https://doi.org/10.1186/s12896-014-0105-9.
[14] A.B. Di Stefano, et al., Cell quality evaluation with gene expression analysis of spheroids (3D) and adherent (2D) adipose stem cells, Gene 768 (2021) 145269.
[15] E. Park, A.N. Patel, Changes in the expression pattern of mesenchymal and pluripotent markers in human adipose-derived stem cells, Cell Biol. Int. 34 (10) (Oct. 2010) 979–984, https://doi.org/10.1042/cbi20100124.
[16] I.N. Saburina, et al., Induction of Vasculo- and osteogenesis in spheroids formed by adipose-derived stromal cells, Bull. Exp. Biol. Med. 166 (1) (Nov. 2018) 163–169, https://doi.org/10.1007/s10517-018-4306-4.
[17] G. Giunta, et al., Identification and expansion of adipose stem cells with enhanced bone regeneration properties, J Regen Med 5 (1) (2015).
[18] A.B. Di Stefano, et al., Human spheroids from adipose-derived stem cells induce calvarial bone production in a xenogeneic rabbit model, Ann. Plast. Surg. 86 (6) (2021) 714–720.
[19] F. Toia, et al., An analysis of the immunomodulatory properties of human spheroids from adipose-derived stem cells, Life Sci. 321 (2023) 121610.
[20] J. Liu, L. Yang, K. Liu, F. Gao, Hydrogel Scaffolds in Bone Regeneration: Their Promising Roles in Angiogenesis, Frontiers Media S.A., 2023, https://doi.org/10.3389/fphar.2023.1050954.
[21] K. Guillén-Carvajal, B. Valdez-Salas, E. Beltrán-Partida, J. Salomón-Carlos, N. Cheng, Chitosan, Gelatin, and Collagen Hydrogels for Bone Regeneration, Multidisciplinary Digital Publishing Institute (MDPI), Jul. 01, 2023, https://doi.org/10.3390/polym15132762.
[22] T.T. Demirtaş, G. Irmak, M. Gümüşderelioğlu, A bioprintable form of chitosan hydrogel for bone tissue engineering, Biofabrication 9 (3) (Jul. 2017), https://doi.org/10.1088/1758-5090/aa7b1d.
[24] B. Sheokand, M. Vats, A. Kumar, C.M. Srivastava, I. Bahadur, S.R. Pathak, Natural polymers used in the dressing materials for wound healing: Past, present and future, J. Polym. Sci. 61 (14) (2023) 1389–1414.
[25] H. Zhong, et al., Near-field electrospun PCL fibers/GelMA hydrogel composite dressing with controlled deferoxamine-release ability and retiform surface for diabetic wound healing, Nano Res. 16 (1) (Jan. 2023) 599–612, https://doi.org/10.1007/s12274-022-4813-5.
[26] I. Fasolino, et al., Osteoinductive and anti-inflammatory properties of chitosan-based scaffolds for bone regeneration, Mater. Sci. Eng. C 105 (Dec. 2019), https://doi.org/10.1016/j.msec.2019.110046.
[27] P. Gupta, S. Sharma, S. Jabin, S. Jadoun, Chitosan nanocomposite for tissue engineering and regenerative medicine: a review, Int. J. Biol. Macromol. 254 (2024) 127660, https://doi.org/10.1016/j.ijbiomac.2023.127660.
[28] J. Nilsen-Nygaard, S. P. Strand, K. M. Vårum, K. I. Draget, and C. T. Nordgård, "Chitosan: Gels and Interfacial Properties," 2015, MDPI AG. doi: https://doi.org/10.3390/polym7030552.
[29] S. Maiz-Fernández, L. Pérez-álvarez, U. Silván, J. L. Vilas-Vilela, and S. Lanceros-Méndez, "pH-induced 3D printable chitosan hydrogels for soft actuation," Polymers (Basel), vol. 14, no. 3, Feb. 2022, doi: https://doi.org/10.3390/polym14030650.
[30] E. Avazverdi, H. Mirzadeh, M. Ehsani, S. Bagheri-Khoulenjani, Polysaccharide-based polyampholyte complex formation: Investigating the role of intra-chain interactions, Carbohydrate Polymers 313 (2023) 120836.
[31] X. Bai, M. Gao, S. Syed, J. Zhuang, X. Xu, X.Q. Zhang, Bioactive Hydrogels for Bone Regeneration, KeAi Communications Co., Dec. 01, 2018, https://doi.org/10.1016/j.bioactmat.2018.05.006.
[32] A.K. Gaharwar, N.A. Peppas, A. Khademhosseini, Nanocomposite hydrogels for biomedical applications, Biotechnol. Bioeng. 111 (2014) 441–453, https://doi.org/10.1002/bit.25160/abstract.
[33] H. Li, K.A. Khor, V. Chow, P. Cheang, Nanostructural characteristics, mechanical properties, and osteoblast response of spark plasma sintered hydroxyapatite, J. Biomed. Mater. Res. A 82 (2) (Aug. 2007) 296–303, https://doi.org/10.1002/jbm.a.31143.
[34] D.V. Abere, S.A. Ojo, G.M. Oyatogun, M.B. Paredes-Epinosa, M.C.D. Niluxsshun, A. Hakami, Mechanical and morphological characterization of nano-hydroxyapatite (nHA) for bone regeneration: a mini review, Biomedical Engineering Advances 4 (Dec. 2022) 100056, https://doi.org/10.1016/j.bea.2022.100056.
[35] J. Venkatesan, S.K. Kim, Nano-Hydroxyapatite Composite Biomaterials for Bone Tissue Engineering - A Review, American Scientific Publishers, 2014, https://doi.org/10.1166/jbn.2014.1893.
[36] M. Rajula, V. Narayanan, G. Venkatasubbu, R. Mani, and A. Sujana, "Nano-Hydroxyapatite: A Driving Force for Bone Tissue Engineering," Jun. 01, 2021, Wolters Kluwer Medknow Publications. doi: https://doi.org/10.4103/jpbs.JPBS_683_20.
[37] S. Dhivya, S. Saravanan, T.P. Sastry, N. Selvamurugan, Nanohydroxyapatite-reinforced chitosan composite hydrogel for bone tissue repair in vitro and in vivo, J Nanobiotechnology 13 (1) (Jun. 2015), https://doi.org/10.1186/s12951-015-0099-z.
[38] Y. Zhang, J.R. Venugopal, A. El-Turki, S. Ramakrishna, B. Su, C.T. Lim, Electrospun biomimetic nanocomposite nanofibers of hydroxyapatite/chitosan for bone tissue engineering, Biomaterials 29 (32) (Nov. 2008) 4314–4322, https://doi.org/10.1016/j.biomaterials.2008.07.038.
[39] J.G. Dellinger, J. Cesarano, R.D. Jamison, Robotic deposition of model hydroxyapatite scaffolds with multiple architectures and multiscale porosity for bone tissue engineering, J. Biomed. Mater. Res. A 82 (2) (Aug. 2007) 383–394, https://doi.org/10.1002/jbm.a.31072.
[40] V. Bakhshi, H. Poursadegh, M.S. Amini-Fazl, D. Salari, S. Javanbakht, Synthesis and characterization of bio-nanocomposite hydrogel beads based on magnetic hydroxyapatite and chitosan: a pH-sensitive drug delivery system for potential implantable anticancer platform, Polymer Bulletin 81 (8) (2024) 7499–7518.
[41] H. Shi, Z. Zhou, W. Li, Y. Fan, Z. Li, J. Wei, Hydroxyapatite based materials for bone tissue engineering: a brief and comprehensive introduction, Crystals (Basel) 11 (2) (Feb. 2021) 149, https://doi.org/10.3390/cryst11020149.
[42] Y. He, Y. Dong, F. Cui, X. Chen, R. Lin, Ectopic osteogenesis and scaffold biodegradation of nano-hydroxyapatite-chitosan in a rat model, PLoS One 10 (8) (Aug. 2015), https://doi.org/10.1371/journal.pone.0135366.
[43] L. Kong, Y. Gao, G. Lu, Y. Gong, N. Zhao, X. Zhang, A study on the bioactivity of chitosan/nano-hydroxyapatite composite scaffolds for bone tissue engineering, Eur. Polym. J. 42 (12) (Dec. 2006) 3171–3179, https://doi.org/10.1016/j.eurpolymj.2006.08.009.
[44] A. Polini, D. Pisignano, M. Parodi, R. Quarto, S. Scaglione, Osteoinduction of human mesenchymal stem cells by bioactive composite scaffolds without supplemental osteogenic growth factors, PLoS One 6 (10) (2011) e26211, https://doi.org/10.1371/journal.pone.0026211.
[45] A. Polini, J. Wang, H. Bai, Y. Zhu, A.P. Tomsia, C. Mao, Stable biofunctionalization of hydroxyapatite (HA) surfaces by HA-binding/osteogenic modular peptides for inducing osteogenic differentiation of mesenchymal stem cells, Biomater. Sci. 2 (2014) 1779–1786, https://doi.org/10.1039/C4BM00164H.
[46] X.G. Tang, M. Hou, J. Zou, R. Truss, Effect of nano-filler network on the rheological behaviours of poly(vinylidene fluoride) nanocomposites, Adv. Mater. Res. (2011) 1232–1238, https://doi.org/10.4028/www.scientific.net/AMR.328-330.1232.
[47] R. Arrigo, E. Morici, N.T. Dintcheva, High-performance thermoplastic elastomers/carbon nanotubes nanocomposites: mechanical behavior, rheology, and durability, Polym. Compos. 38 (2017) E381–E391.
[48] P. Coussot, Introduction to the rheology of complex fluids, in: Understanding the Rheology of Concrete, Elsevier, 2012, pp. 3–22, https://doi.org/10.1533/9780857095282.1.3.
[49] A.S. Sarvestani, E. Jabbari, Modeling the viscoelastic response of suspension of particles in polymer solution: the effect of polymer-particle interactions, Macromol. Theory Simul. 16 (4) (May 2007) 378–385, https://doi.org/10.1002/mats.200700009.
[50] J. Adhikari, Md.S. Perwez, A. Das, P. Saha, Development of hydroxyapatite reinforced alginate–chitosan based printable biomaterial-ink, Nano-Structures & Nano-Objects 25 (2021) 100630, https://doi.org/10.1016/j.nanoso.2020.100630.
[51] C. Yan, D.J. Pochan, Rheological properties of peptide-based hydrogels for biomedical and other applications, Chem. Soc. Rev. 39 (9) (2010) 3528–3540.
[52] B. Y. S. Kumar, A. M. Isloor, G. C. M. Kumar, Inamuddin, and A. M. Asiri, "Nanohydroxyapatite reinforced chitosan composite hydrogel with tunable mechanical and biological properties for cartilage regeneration," Sci. Rep., vol. 9, no. 1, Dec. 2019, doi: https://doi.org/10.1038/s41598-019-52042-7.
[53] M.J. Moura, M.M. Figueiredo, M.H. Gil, Rheological study of genipin cross-linked chitosan hydrogels, Biomacromolecules 8 (12) (Dec. 2007) 3823–3829, https://doi.org/10.1021/bm700762w.
[54] Y. Tang, X. Wang, B. Huang, Z. Wang, N. Zhang, Effect of cationic surface modification on the rheological behavior and microstructure of nanocrystalline cellulose, Polymers (Basel) 10 (3) (Mar. 2018), https://doi.org/10.3390/polym10030278.
[55] M.R. Nikpour, S.M. Rabiee, M. Jahanshahi, Synthesis and characterization of hydroxyapatite/chitosan nanocomposite materials for medical engineering applications, Compos B Eng 43 (4) (Jun. 2012) 1881–1886, https://doi.org/10.1016/j.compositesb.2012.01.056.
[56] R. Rial, J.F.A. Soltero, P.V. Verdes, Z. Liu, J.M. Ruso, Mechanical properties of composite hydrogels for tissue engineering, Curr. Top. Med. Chem. 18 (14) (Aug. 2018) 1214–1223, https://doi.org/10.2174/1568026618666180810151539.
[57] Z. Bao, Z. Gu, J. Xu, M. Zhao, G. Liu, J. Wu, Acid-responsive composite hydrogel platform with space-controllable stiffness and calcium supply for enhanced bone regeneration, Chem. Eng. J. 396 (Sep. 2020), https://doi.org/10.1016/j.cej.2020.125353.
[58] B. Zhao, et al., Preparation and properties of double-crosslinked hydroxyapatite composite hydrogels, Int. J. Mol. Sci. 23 (17) (Sep. 2022), https://doi.org/10.3390/ijms23179962.
[60] M. Qin, et al., High-strength, fatigue-resistant, and fast self-healing antibacterial nanocomposite hydrogels for wound healing, Chem. Eng. J. 455 (Jan. 2023), https://doi.org/10.1016/j.cej.2022.140854.
[61] X. Gao, Z. Shi, C. Liu, G. Yang, I. Sevostianov, V.V. Silberschmidt, Inelastic behaviour of bacterial cellulose hydrogel: in aqua cyclic tests, Polym. Test. 44 (Jul. 2015) 82–92, https://doi.org/10.1016/j.polymertesting.2015.03.021.
[63] J. Grenier, H. Duval, F. Barou, P. Lv, B. David, D. Letourneur, Mechanisms of pore formation in hydrogel scaffolds textured by freeze-drying, Acta Biomater. 94 (Aug. 2019) 195–203, https://doi.org/10.1016/j.actbio.2019.05.070.
[65] Z. Emami, M. Ehsani, M. Zandi, H. Daemi, M.H. Ghanian, R. Foudazi, Modified hydroxyapatite nanoparticles reinforced nanocomposite hydrogels based on gelatin/oxidized alginate via Schiff base reaction, Carbohydrate Polymer Technologies and Applications 2 (Dec. 2021), https://doi.org/10.1016/j.carpta.2021.100056.
[66] U. Sabu, G. Logesh, M. Rashad, A. Joy, M. Balasubramanian, Microwave assisted synthesis of biomorphic hydroxyapatite, Ceram. Int. 45 (6) (Apr. 2019) 6718–6722, https://doi.org/10.1016/j.ceramint.2018.12.161.
[67] R. N. Panda, M. F. Hsieh, R. J. Chung, and T. S. Chin, "FTIR, XRD, SEM and solid state NMR investigations of carbonate-containing hydroxyapatite nano-particles

synthesized by hydroxide-gel technique." [Online]. Available: www.elsevier.com/locate/jpcs.
[68] A. Rogina, et al., Cellular hydrogels based on pH-responsive chitosan-hydroxyapatite system, Carbohydr. Polym. 166 (Jun. 2017) 173–182, https://doi.org/10.1016/j.carbpol.2017.02.105.
[69] N. Rameshbabu, K.P. Rao, T.S.S. Kumar, Acclerated microwave processing of nanocrystalline hydroxyapatite, J. Mater. Sci. 40 (23) (Dec. 2005) 6319–6323, https://doi.org/10.1007/s10853-005-2957-9.
[70] K. Thirupathi, et al., Update on Chitosan-based Hydrogels: Preparation, Characterization, and Its Antimicrobial and Antibiofilm Applications, MDPI, Jan. 01, 2023, https://doi.org/10.3390/gels9010035.
[71] F. Lopresti, F. Carfì Pavia, I. Vitrano, M. Kersaudy-Kerhoas, V. Brucato, V. La Carrubba, Effect of hydroxyapatite concentration and size on morpho-mechanical properties of PLA-based randomly oriented and aligned electrospun nanofibrous mats, J. Mech. Behav. Biomed. Mater. 101 (Jan. 2020), https://doi.org/10.1016/j.jmbbm.2019.103449.
[72] E. Elline, K. Ismiyatin, and T. I. Budhy, "Novel biodegradable hydrogel scaffold based on hydroxyapatite eggshell, collagen, and epigallocatechin-3-gallate," 2023. [Online]. Available: www.ncbi.nlm.nih.gov/pmc/journals/1480.
[73] J. Triyono, R. Adityawan, P. Dananjaya, D.F. Smaradhana, A. Masykur, Characterization and biodegradation rate of hydroxyapatite/shellac/sorghum for bone scaffold materials, Cogent Eng 8 (1) (2021), https://doi.org/10.1080/23311916.2021.1884335.
[74] B. Kaczmarek, et al., In vivo study on scaffolds based on chitosan, collagen, and hyaluronic acid with hydroxyapatite, Int. J. Biol. Macromol. 118 (Oct. 2018) 938–944, https://doi.org/10.1016/j.ijbiomac.2018.06.175.
[75] Z. Bao, C. Xian, Q. Yuan, G. Liu, and J. Wu, "Natural Polymer-based Hydrogels With Enhanced Mechanical Performances: Preparation, Structure, and Property," Sep. 01, 2019, Wiley-VCH Verlag. doi: https://doi.org/10.1002/adhm.201900670.
[77] G. Fletes-Vargas, et al., Porous chitosan hydrogels produced by physical crosslinking: physicochemical, structural, and cytotoxic properties, Polymers (Basel) 15 (9) (May 2023) 2203, https://doi.org/10.3390/polym15092203.
[78] N. Annabi, et al., Controlling the Porosity and Microarchitecture of Hydrogels for Tissue Engineering, Aug. 01, 2010, https://doi.org/10.1089/ten.teb.2009.0639.
[79] A. Soriente, et al., Chitosan/hydroxyapatite nanocomposite scaffolds to modulate osteogenic and inflammatory response, J. Biomed. Mater. Res. A 110 (2) (Feb. 2022) 266–272, https://doi.org/10.1002/jbm.a.37283.
[80] A. Rogina, et al., Human mesenchymal stem cells differentiation regulated by hydroxyapatite content within chitosan-based scaffolds under perfusion conditions, Polymers (Basel) 9 (9) (Aug. 2017) 387, https://doi.org/10.3390/polym9090387.
[81] S. Sundelacruz, D.L. Kaplan, Stem cell- and scaffold-based tissue engineering approaches to osteochondral regenerative medicine, Semin. Cell Dev. Biol. 20 (6) (Aug. 2009) 646–655, https://doi.org/10.1016/j.semcdb.2009.03.017.
[82] J. Sodek, et al., Regulation of osteopontin expression in osteoblasts, Ann. N. Y. Acad. Sci. 760 (1) (Aug. 1995) 223–241, https://doi.org/10.1111/j.1749-6632.1995.tb44633.x.
[83] M. Inoue, M.L. Shinohara, Intracellular osteopontin (iOPN) and immunity, Immunol. Res. 49 (1–3) (Apr. 2011) 160–172, https://doi.org/10.1007/s12026-010-8179-5.
[84] J. Grzesiak, A. Śmieszek, K. Marycz, Ultrastructural changes during osteogenic differentiation in mesenchymal stromal cells cultured in alginate hydrogel, Cell Biosci. 7 (2017) 2, https://doi.org/10.1186/s13578-016-0128-0.